Article

Particle Image Velocimetry Measurements of the Flow-Diverting Effects of a New Generation of the eCLIPs Implant for the Treatment of Intracranial Bifurcation Aneurysms

Sina G. Yazdi [1],*, Daniel Mercier [1], Renee Bernard [1], Adam Tynan [1] and Donald R. Ricci [1,2]

[1] Evasc Medical Systems, Vancouver, BC V6H 1C3, Canada; mercier@evasc.com (D.M.); bernard@evasc.com (R.B.); tynan@evasc.com (A.T.); ricci@mail.ubc.ca (D.R.R.)

[2] Department of Medicine, University of British Columbia, Vancouver, BC V5Z 1M9, Canada

* Correspondence: yazdi@evasc.com

check for updates

Abstract: Flow diverters (FDs) for the endovascular treatment of intracranial aneurysms are effective for sidewall aneurysms, but their use at a bifurcation is problematic because FDs only partially cover the aneurysm neck and impede flow into a daughter branch; they are thus not employed routinely in this anatomy. eCLIPs was developed as a non-tubular implant to completely cover the neck of an aneurysm and serve as a coil retention device necessary for the adequate treatment of wide-neck bifurcation aneurysms. eCLIPs has shown some flow diversion effects in bifurcation anatomy but not equal to those exhibited by clinically accepted flow diverters in sidewall anatomy. A new generation of eCLIPs implant, the eCLIPs bifurcation flow diverter (eBFD), with higher metal coverage, was developed to achieve a similar flow diversion as a Pipeline Embolization Device (PED), a prototypical FD. Particle image velocimetry was used to capture the fluid dynamics and velocity reduction within silicone aneurysm replicas. A circulatory mimicking loop was developed to circulate the flow through the silicone models. All generations of eCLIPs implants had some flow-diverting effect, with increasing metal coverage density of the implant proportionately increasing the flow diversion effect. The eBFD, with a metal density of 35%, showed greater flow diversion than PED, with 30% metal density, for bifurcation anatomy. The eBFD showed similar reduction of flow in a bifurcation anatomy to PED in a sidewall, both sufficient to permit early thrombosis of the aneurysm. Thus, the eBFD can potentially provide sufficient flow diversion for the treatment of bifurcation aneurysms to avoid adjunctive coiling.

Keywords: particle image velocimetry; flow diverter; aneurysm; bifurcation; hemodynamic; velocity reduction; coil
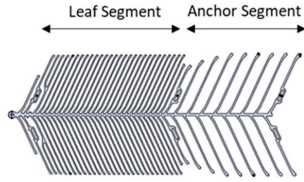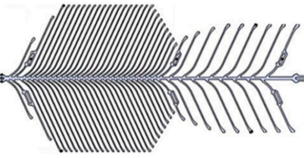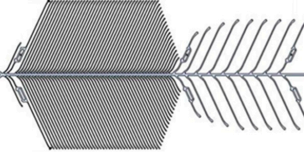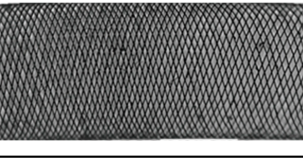
1. Introduction

A brain aneurysm is a localized enlargement of an intracranial artery, usually due to damaged smooth muscle cells and elastin in the arterial layers [1] but often exacerbated by localized perturbation of blood flow. The Brain Aneurysm Foundation reported that the worldwide annual mortality due to intracranial aneurysms is 500,000, with approximately 50% of these patients being younger than 50 years old [2]. Common treatments for intracranial aneurysms include embolic coiling and stent-assisted coiling, but these are associated with frequent recurrence, especially for wide-neck aneurysms [3,4]. Stent-assisted coiling prevents coil protrusion into the parent artery lumen, a particular problem with wide-neck aneurysms, and reduces the recurrence risk [5]. Intra-aneurysmal coils act by initiating and propagating thrombus that ultimately cause the aneurysm to heal by thrombotic occlusion.

An emerging method to treat brain aneurysms is the use of flow diverter (FD) devices. Typically, FDs are tubular stents made of high-density braided mesh that minimizes blood perfusion through the stent wall into the aneurysm, producing blood stasis within the aneurysm that facilitates thrombus and thereby mitigates the need for coils [6]. All available FD devices in the market are designed for the treatment of sidewall aneurysms, but many aneurysms occur at a bifurcation. Y stenting is occasionally performed at a bifurcation to secure the coil and provide better neck coverage by deploying one stent from the parent artery to one daughter branch and then telescoping a second stent to the other (contralateral) branch [7,8]. FDs are not well suited to this anatomy because delivery methods preclude complete bridging of the neck. A FD is implanted from the parent artery to one daughter branch, providing a "neck narrowing" function to retain coils while also partially redirecting flow away from the aneurysm. Both Y stenting and FDs result in only partial coverage of the neck of the bifurcation, impede access to side branches, and, in the case of FDs, reduce the flow into contralateral side branches with the risk of hypoperfusion [9]. Another method for treating intracranial bifurcation aneurysms is with intrasaccular devices (e.g., WEB, Woven EndoBridge, Microvention, Aliso Viejo, CA, USA) [10]. While these devices disrupt intrasaccular flow to initiate thrombus, they do not reduce flow entering the neck of the aneurysm, a factor that can result in shape modification and compaction of intrasaccular contents [11,12].

eCLIPs (eCLIPs[TM], eVasc Neurovascular, Vancouver, BC, Canada) implants are semi-circumferential but non-tubular devices with two sections (Table 1): an anchor segment that is placed into one branch, and a leaf segment that crosses the neck of a bifurcation from one side branch to the other (contralateral) to effect coil retention without blocking the flow to the branches [13]. Peach et al. [14] demonstrated the FD characteristics of the eCLIPs leaf section using computational flow dynamics (CFD). They compared the eCLIPs flow diversion against that of clinically accepted FDs, e.g., the Pipeline Embolization Device (PED, Medtronic, Minneapolis, MN, USA), in a bifurcation geometry. They concluded that eCLIPs is 10% less effective than braided mesh in reducing the inflow and the jet into the aneurysm, possibly due to the larger pore size, but does not impede flow into either side branch. Different numerical and experimental hemodynamic studies had shown that reducing the pore size leads to a greater flow diversion effect [15–17]. Particle image velocimetry (PIV) is an optical measurement technique that has been widely used for in vitro assessment of the intracranial aneurysm hemodynamics and flow diversion effect [16–18].

The current state of the art in the endovascular treatment of intracranial aneurysms does not offer a universally reliable and safe method to treat bifurcation aneurysms but suggests that FDs in some form may offer a solution. The eCLIPs implant has had three iterations: an early "proof of principle" stainless steel version [19] and two nitinol versions, the earlier (eCLIPs bifurcation remodelling system, eBRS) having FD characteristics as described by Peach et al. [14] and the later having improved deliverability (eCLIPs electrolytic bifurcation, eB) [20]. A fourth generation of eCLIPs implant (eCLIPs bifurcation flow diverter, eBFD) was developed with increased metal coverage (density) to enhance the flow diversion effect of the eCLIPs implants at a bifurcation. The objective of this study was to use PIV to assess the degrees of flow diversion of the successive generations of eCLIPs implant, particularly the fourth generation (eBFD), and to compare the results against those of a clinically accepted FD, PED (Table 1), which was tested in a sidewall and bifurcation aneurysm configuration. Enhanced flow diversion by the eBFD may be sufficient for healing a bifurcation aneurysm without the need for adjunctive coiling.

Table 1. Illustration and general characteristics of the three versions of eCLIPs and Pipeline studied using particle image velocimetry (PIV) analysis; the Pipeline device image was adapted from Dholakia et al. [21].

Series	Implant Figure		Metal Coverage (Density)	Common Geometry Implanted	Purpose of Use
eCLIPs Series		**eBRS**	26%	Bifurcation aneurysm	Coil retention
		eB	21%	Bifurcation aneurysm	Coil retention
		eBFD	35%	Bifurcation aneurysm	Flow diversion
Pipeline (PED)			30%	Sidewall aneurysm	Flow diversion

2. Materials and Methods

Two arterial phantoms were used in this study. First, an idealized 1:1 scale compliant phantom of the basilar artery with posterior cerebral branches was designed with an aneurysm at the bifurcation (Figure 1a). Another 1:1 scale model of the basilar artery with a sidewall aneurysm was designed (Figure 1b). The phantoms were manufactured from Silicone Sylgard-184 (Dow Corning Inc. Midland, MI, USA) at room temperature (23 °C) (Figure 1c). The lost core casting method developed by Yazdi et al. [22] was used for phantoms manufacture; the details of the moulding process can be found in their study. It was reported that the Sylgard-184 has a Young's modulus of 1.32 MPa if it is cured at room temperature [23,24]; thus, it was not measured in this study.

In total, 7 experiments were conducted and 4 implants were tested. Cases 2 and 3 (generations 2 and 3) were eCLIPs coil assisting implants commercially available on the market. Case 4 (generation 4) was a revision developed with higher metal coverage. A schematic view of an eCLIPs implant in bifurcation configuration is shown in Figure 2a. Since the PED implant is the prototypical FD, its measure of flow diversion was used as a reference to compare the eCLIPs' results. The PED was implanted in both bifurcation (Case 5) (Figure 2b) and sidewall (Case 7) configurations (Figure 2c). Cases 1 and 6 were the silicone models without any implant and served as baselines to assess the flow diversion effect.
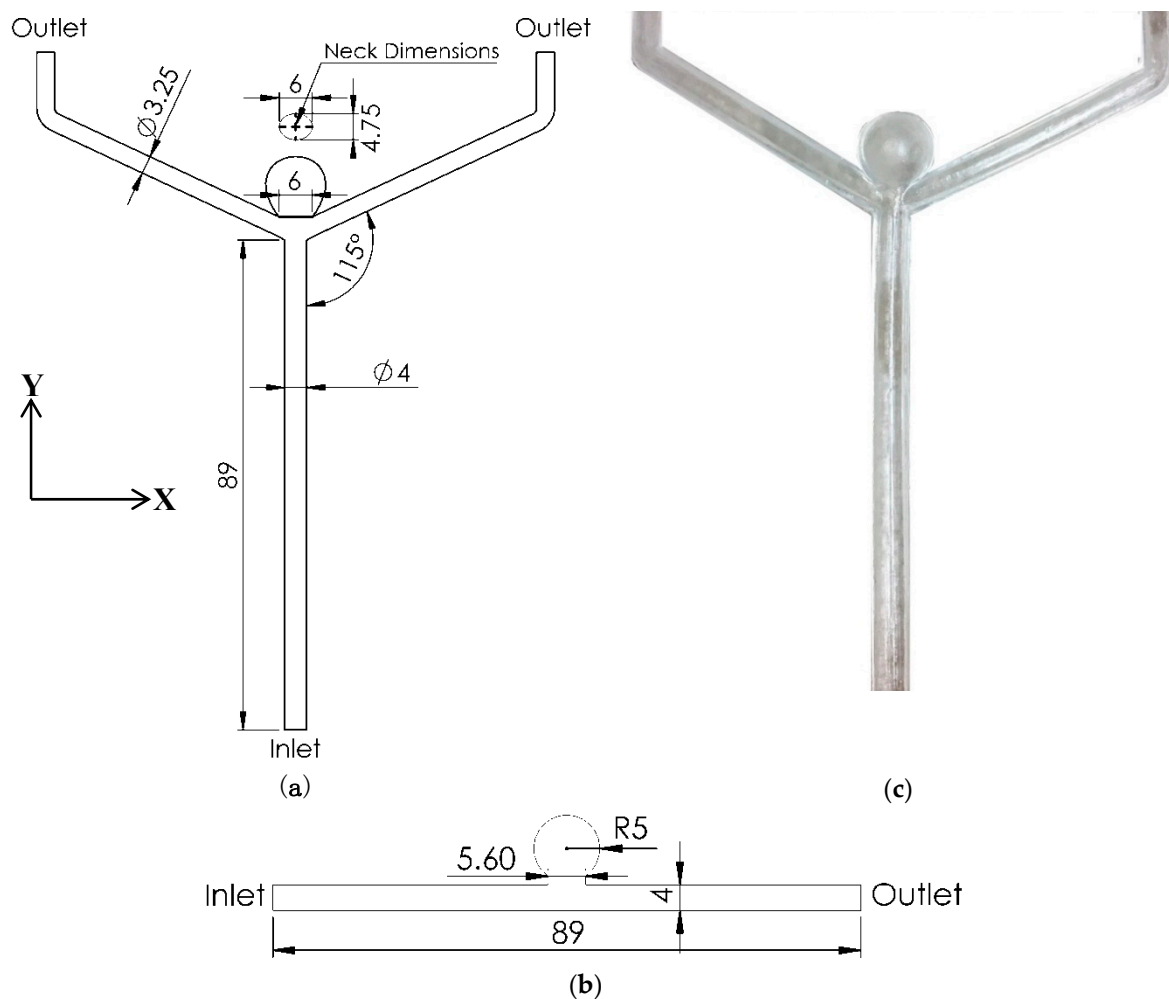
Figure 1. (**a**) Bifurcation aneurysm model drawing, (**b**) sidewall model drawing, and (**c**) sample image of the manufactured silicone model; length units are in mm.

A fluid circuit was developed to run the flow through the phantoms (Figure 3). A solution of 47.38% water, 36.94% glycerine, and 15.68% sodium iodide was used as a blood analogue [25]. The circuit consisted of a steady pump, magnetic-inductive flowmeter (SM 4000, IFM Inc., Daimlerring, Germany), phantom box, reservoir, and header tank. The header tank was used to mimic the impedance of the smaller arteries and capillaries. To eliminate the vibration in the fluid line and aneurysm due to the pump propulsion, the fluid was pumped to a reservoir (Figure 3) and gravity-fed to the model. A weir was designed in the reservoir to keep the fluid level constant. To eliminate optical distortion during the PIV experimentation, the working fluid should have the same refractive index as the silicone phantoms. The phantom box was also filled with the same working fluid to mimic the surrounding tissue. This solution matched the refractive index of the silicone Sylgar-184 (n = 1.414), which was verified by placing a checkerboard behind the phantom and capturing images to check for distortion of the grids. The solution had dynamic viscosity of 4.31 cP, which is in the range of human blood viscosity [25]. The volumetric flow rate in the basilar artery can reach up to 300 mL/min at peak systole [17,26]. Since it was expected to see the highest velocity and blood protrusion into the aneurysm at peak systole, all the experiments were conducted at a 300 mL/min steady flow. Since there are no published data on the shear rate threshold for successful flow diversion and thrombosis formation in a bifurcation aneurysm, the current study only mapped the velocity field in the aneurysm sac and discussed the flow diversion based on the velocity reduction.
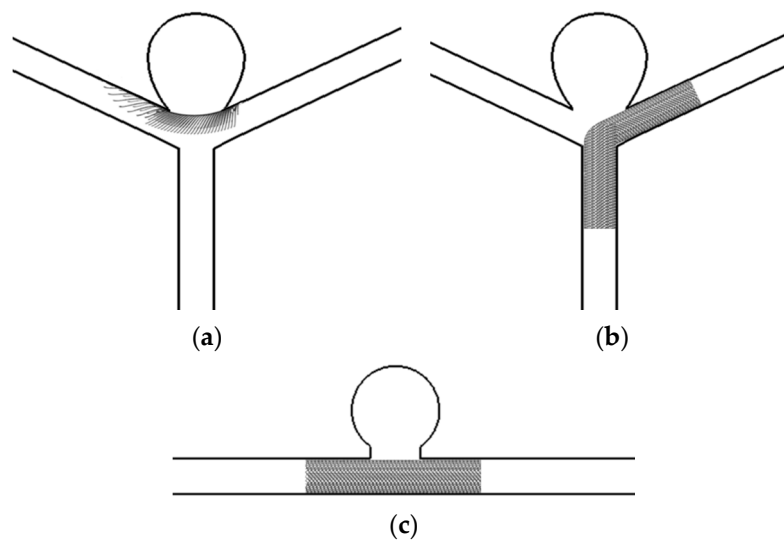
Figure 2. Schematic views of the deployed implants in different configurations: (**a**) eCLIPs in bifurcation, (**b**) PED in bifurcation, and (**c**) PED in sidewall configuration.
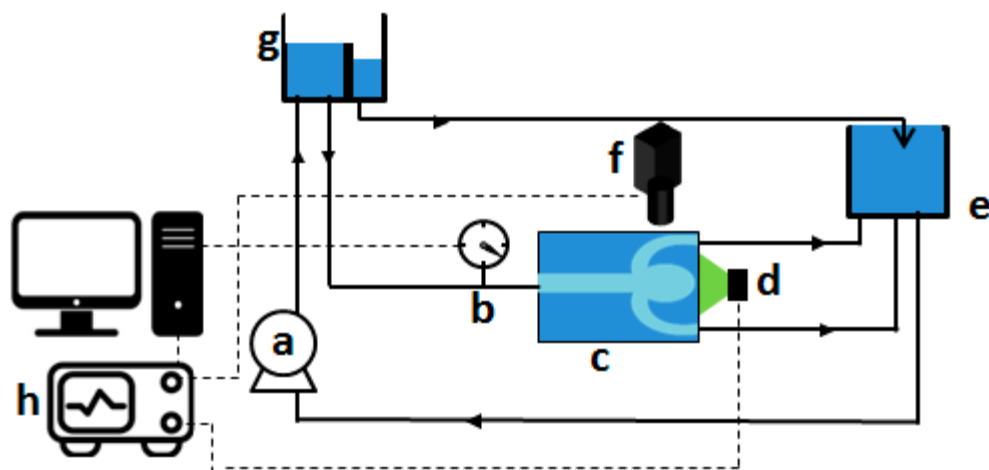

Figure 3. Schematic view of the fluid circuit and PIV setup: (**a**) steady pump, (**b**) magnetic-inductive flowmeter, (**c**) phantom box, (**d**) LED light source, (**e**) header tank, (**f**) PIV camera, (**g**) reservoir (header tank with weir), (**h**) control platform.

Planar PIV was used to capture the fluid dynamics within the aneurysm dome. A high-power LED (ILA-5150 GmbH, Aachen, Germany) light source was used to illuminate the region of interest. Fiber optics connected to the LED head transferred the illumination to the light sheet generator composed of cylindrical lenses. The adjusted light sheet had a thickness of 1 mm and was aligned with the central coronal plane of the aneurysm for which all the results were captured. An ILA μEYE PIV camera (ILA-5150 GmbH, Aachen, Germany) with 2048 × 2048 pixels was used to capture the particle images. The camera was equipped with a 35 mm lens installed on a 40 mm C-mount extension. This allowed the lens to focus on objects at shorter distances than would be possible without a spacer, thus increasing the magnification of the image on the camera sensor. The flow was seeded polyamide particles with a nominal diameter of 5 μm. An ILA network synchronizer was used to fire the LED in double-pulsed mode and synchronize the illumination and capture events.

Light reflection from the silicone model wall and stationary objects can cause an error in displacement vector calculation. Thus, to increase the signal-to-noise ratio before cross-correlation, the average intensity background was subtracted from the images. Gaussian window weighting was

applied to images prior to the correlation. Preprocessing of the images eliminated the peak-locking effect, which is a cause of bias in the PIV analysis and increases the velocity uncertainty. Cross-correlation was used to compute the displacement vector field. For all analyses, 100 image pairs were captured and used for the analysis of the ensemble-averaged vector field. Almost no interpolated vector was observed in the ensemble averaged vector field. A combination of the mentioned conditions ensured low uncertainty of the calculated velocity field. Iterative window refinement was used for grid generation with start and final window dimensions of 225 × 225 and 48 × 48 pixels, respectively, with 50% grid overlapping. Normalized median testing of the 8 neighboring grids was used to validate the computed vector field. PIVview2C software was used for the analysis of the images. The mapped velocity data were plotted using Tecplot 360 software.

3. Results

Figure 4 shows the velocity contour plots of all cases with and without implants in bifurcation and sidewall configurations. Due to the difference in peak velocity between the control case and the cases with implants, a logarithmic scale color map was used to enhance the comparison. In general, the figures show the effect of higher metal coverage on flow diversion by progressively reducing velocity within the aneurysm.
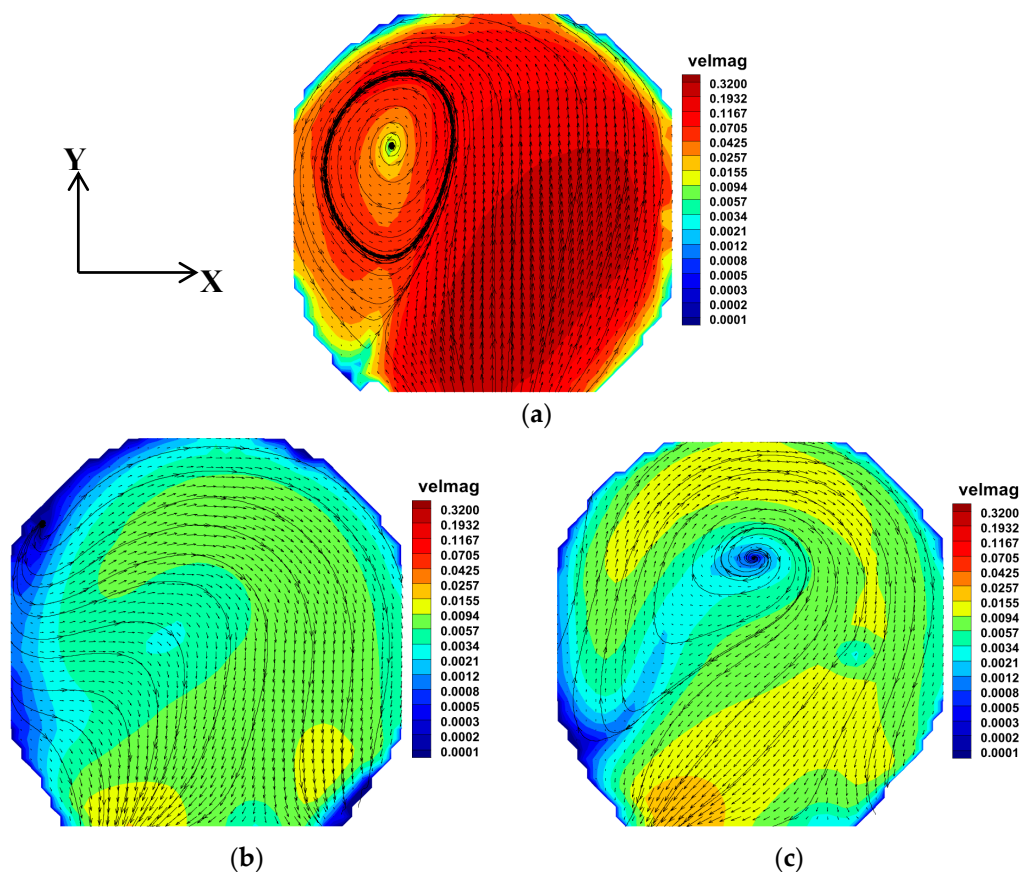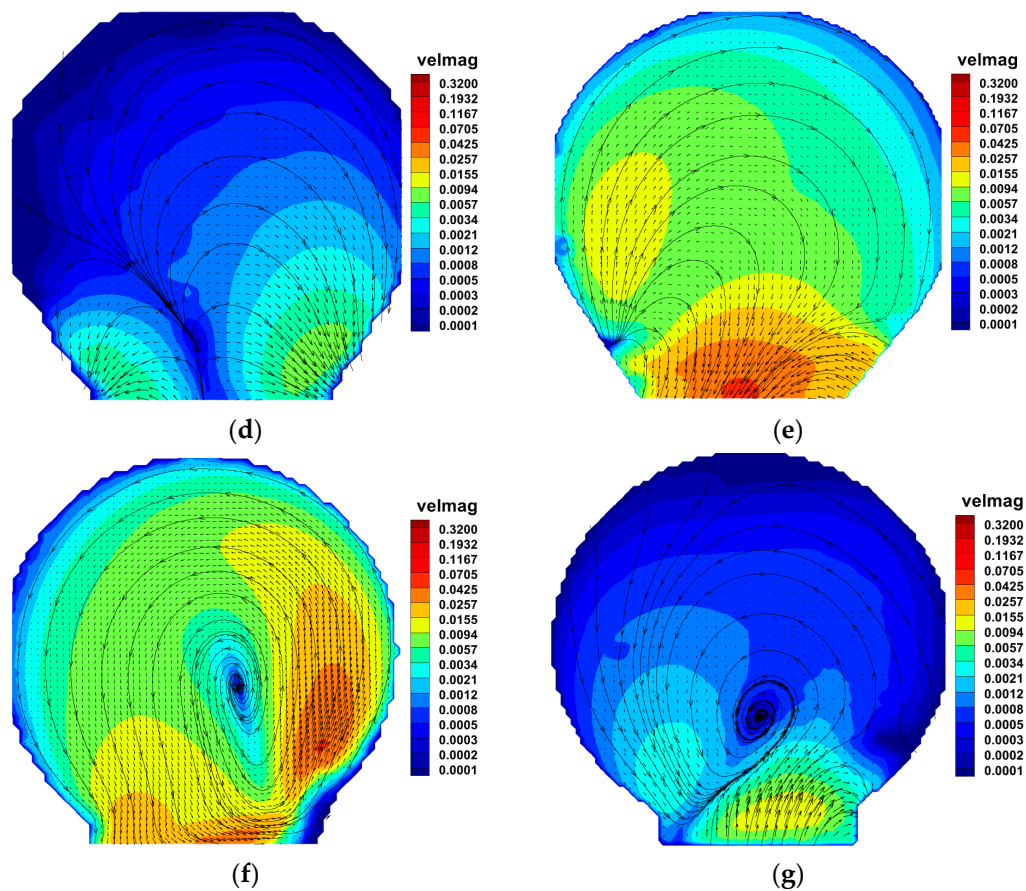

Figure 4. *Cont.*

Figure 4. Velocity colour mapping and flow streamlines for different implants in sidewall and bifurcation geometry; note that logarithmic color mapping was used to enhance the comparison of contours. (**a**) Case 1, bifurcation, no implant, (**b**) Case 2, bifurcation, eBRS, (**c**) Case 3, bifurcation, eB, (**d**) Case 4, bifurcation, eBFD, (**e**) Case 5, bifurcation, PED, (**f**) Case 6, sidewall, no implant, (**g**) Case 7, sidewall, PED.

Table 2 shows the mean and maximum velocity measurements for each case and the percentage of reduction compared with the control case. As the metal coverage density increases, the mean and maximum velocities are reduced. The highest velocity reduction was observed in Case 4, the eCLIPs fourth-generation eBFD, which had the highest density.

Table 2. Peak and average aneurysm velocities and the percentage of reduction for each case at 300 mL/min volumetric flow rate.

Case	Density%	Max. Velocity (m/s)	Max Velocity Reduction (%)	Mean Velocity (m/s)	Mean Velocity Reduction (%)
Bifurcation					
Case 1, no implant	N/A	0.320	N/A	0.127	N/A
Case 2, eBRS (Generation 2)	26	0.0172	95	0.0049	96
Case 3, eB (Generation 3)	21	0.0260	92	0.0077	94
Case 4, eBFD (Generation 4)	35	0.0100	97	0.0014	98
Case 5, PED 3.75 mm × 18 mm	30	0.0380	88	0.0075	94
Sidewall					
Case 6, no implant	N/A	0.0500	N/A	0.0096	N/A
Case 7, PED 3.75 mm × 18 mm	30	0.0144	84	0.0013	86

Figure 4a shows the bifurcation aneurysm without an implant (control case). A jet was observed that entered the aneurysm predominantly from the distal end of the neck. The maximum velocity obtained was 0.32 m/s, which is significantly close to the theoretical velocity of 0.39 m/s calculated in the parent artery given the volumetric flow rate and model dimensions stated earlier. A considerable recirculation can be seen in the velocity map, with the core located near the top of the dome. For the eBRS implant (Figure 4b), the velocity was reduced across the dome, and there was no evidence of recirculation. The eB implant (Figure 4c) showed a similar flow pattern to the eBRS. However, a recirculation was observed, relatively weaker than that in the control case. The recirculation was counter-clockwise in the control case, while a clockwise recirculation was observed in the eB case. Amongst all the implants in the bifurcation configuration, the eBFD showed the best flow diversion performance and velocity reduction (Figure 4d). The maximum and mean velocity were reduced by 97% and 98%, respectively (Table 2). The velocity was significantly reduced at the dome, with no evidence of recirculation, and the highest velocity was observed at the sides of the neck.

The PED in the bifurcation geometry (Figure 4e) showed a lesser level of flow diversion than the eBFD, and the mean velocity reduction was the same as that of eB (Table 2). The flow entered the aneurysm from the distal end of the neck with a relatively high core velocity.

In the sidewall geometry without an implant, flow entered the aneurysm from the distal end of the neck, and a jet with a core velocity of 0.05 m/s was observed (Figure 4f). The flow circulated at the center of the aneurysm. Of note is that the velocity entering the aneurysm at the bifurcation location (0.32 m/s, Table 2) was markedly higher than that entering at the sidewall location (0.05 m/s, Table 2). Deployment of the PED in the sidewall configuration (Figure 4g) led to a considerable reduction of the velocity in the aneurysm sac, particularly at the top of the dome. The velocity color mapping showed that the eBFD at a bifurcation (Case 4) resulted in a greater reduction in inflow velocity—mean and maximal velocity reductions of 97% and 98%, respectively—than did the PED at a sidewall (Case 7)—mean and maximal velocity reductions of 84% and 86%, respectively.

4. Discussion

Flow diverters have been accepted as standalone implants for the treatment of intracranial aneurysms in lieu of other conventional treatment methods, including clipping, embolic coil, and stent-assisted coiling, in particular for wide-neck aneurysms [27]. However, effective flow diversion by the implant for aneurysm healing is considerably dependent on the velocity reduction within the aneurysm sac [28]. The current study used a PIV optical fluid dynamics measurement technique to evaluate the flow diversion effect of a new generation of the eCLIPs flow diverter and compare the results to those of previous eCLIPs coil retaining implants and the PED flow diverter.

The deployment of all devices caused a flow-diverting effect in the aneurysm dome. However, the level of flow diversion and reduction of aneurysmal velocity compared with the baseline were different across the implants and configurations. The results showed that there is a strong correlation between metal coverage density and flow reduction. This finding was in agreement with previously published studies [15–17]. For instance, the eBRS and eB implants both reduced the velocity within the aneurysm, with metal densities of 26% and 21%, respectively.

Yu et al. [29] experimentally investigated the effect of stent porosity in reducing cerebral sidewall aneurysm flow using PIV. They reported that to effectively dampen the flow in an aneurysm, the stent porosity should be kept around 60% (40% metal coverage), and for a porosity of 64% (36% metal coverage), the velocity decreased by 98% in the aneurysm [29]. The eBFD was manufactured with 35% metal coverage. It had the highest flow reduction amongst the implants, with a mean flow reduction of 98%, concordant with results by Yu et al. [29]. Their observation that a 26% density yielded a mean velocity of 0.0048 m/s in the aneurysm is comparable to the mean velocity of 0.0049 m/s observed for the eBRS (also 26% density). Thus, Yu's data provide a measure of validity to the results obtained in this report.

A jet and large recirculation was observed in the sidewall anatomy (Figure 4f) with no device across the neck. A computational study by Castro et al. [30] showed similar fluid dynamics in a cerebral bifurcation without an implant at peak systole. As expected, the PED implant in sidewall configuration significantly reduced the flow in the aneurysm dome (Figure 4g)—a result of the high density of the braided mesh influencing the fluid dynamics in the aneurysm dome. The PED has been widely accepted as an effective flow diverter for the treatment of sidewall intracranial aneurysms. A review by Wong et al. [6] of PED flow diverters' clinical outcomes reported that the PED is an effective implant to treat wide-necked, fusiform, large, and giant unruptured aneurysms, with 5% of patients experiencing permanent major morbidity and mortality. However, they emphasized a lack of understanding of the flow diverter's effect at bifurcations.

While the PED has 30% metal coverage, as reported in the device's instruction for use, the PED in the bifurcation configuration showed higher velocity entering the aneurysm (mean velocity 0.0075 m/s) than either the eBRS (0.0049 m/s) or eBFD (0.0014 m/s) and effectively the same as the eB implant (0.0077 m/s) with 21% density (Table 2). The higher PED mean velocity in the bifurcation geometry over a device that fully bridges the neck, such as eCLIPs implants, may be explained by the PED bending at the transition between the parent artery and daughter branch, leading to mesh stretching and higher porosity. In addition, the PED in the bifurcation configuration only partially covers the aneurysm neck, potentially leading to a Venturi effect and high velocity at the neck. While not quantified, visual inspection showed an obvious, and expected, reduction of the outflow into the contralateral branch. This observation was highlighted by Tang et al. [9], who computationally modelled the blood flow in a bifurcation geometry pre- and post-implantation of a PED and showed a reduction of the flow rate into the contralateral branch, leading to hypoperfusion post stenting.

The velocity entering the aneurysm at the bifurcation location is markedly higher than that entering at a sidewall location, as might be expected due to the flow perturbation unique to a bifurcation geometry [11], comporting with the clinical observation that a water jet phenomenon at a bifurcation is the likely cause of the higher rate of recurrence at a bifurcation [31].

The eBFD flow diverter in the bifurcation shows a reduction of mean velocity of 98%, whereas the PED has a mean reduction of mean velocity of 86% in a sidewall configuration. Possibly more importantly, the mean velocity is 0.0014 m/s within a bifurcation aneurysm with an eBFD implant and is 0.0013 m/s for a PED implant at a sidewall. Mut et al. [28], using CFD simulation, studied the association of hemodynamic conditions and occlusion times after flow diversion in cerebral aneurysm. Their study reported that the threshold for early occlusion of the aneurysm (thrombosis at 3 months) is a reduction of aneurysm velocity to 0.013 m/s. Both the eBFD and PED exceeded this threshold in the bifurcation and sidewall locations, respectively, by a factor of 10. Recognizing that the PED is accepted in clinical use as a FD in sidewall applications with a mean velocity of 0.0013 m/s, the eBFD, with an aneurysm mean velocity of 0.0014 m/s, should provide the same security of early thrombus formation in a bifurcation aneurysm as PED confers in a sidewall aneurysm. The successful flow-diverting effect of the eBFD in a bifurcation aneurysm, however, would occur without obstructing the flow into either side branch.

While wall shear stress (WSS) is an important parameter in the analysis of aneurysm flow diversion effects, it was not calculated in this study due to aliasing and light reflection at the lumen wall that may lead to error in the cross-correlation algorithm. CFD analysis can be implemented in the future to calculate the WSS in three dimensions and high resolution. Kim et al. [32] numerically showed that the placement of the stents reduced the velocity and vortices in the aneurysm sac, which caused a reduction of the wall shear stress and shear rate. In the current study, we also observed velocity and recirculation area reductions in the aneurysm after implantation. Since the shear rate and WSS are directly proportional to the velocity gradient, it is expected that the shear rate and WSS stress are reduced, similar to the results by Kim et al. [32].

While blood exhibits non-Newtonian behavior for a shear rate lower than 100 1/s, the working fluid used in this study was Newtonian. Najjari et al. [33] reported that the refractive index of

xanthan-gum-based non-Newtonian fluid cannot be matched easily by varying NaI as it considerably changes the fluid viscosity. Failing to perfectly match the refractive index causes optical distortion in PIV analysis and bias in the cross-correlation algorithm, leading to inaccurate results. Thus, a Newtonian fluid was chosen as a blood analogue. Using a non-Newtonian blood analogue might yield improved outcomes. However, different experimental and numerical hemodynamic studies have used a Newtonian model and proved that it provides a good estimation of flow characteristics [34,35]. Valencia et al. [35] numerically investigated the effect of the non-Newtonian fluid assumption on blood flow dynamics in the internal carotid artery with a saccular aneurysm. The study reported that the non-Newtonian effect on wall shear stress was only important in high-velocity-gradient areas. However, both Newtonian and non-Newtonian models showed similar wall shear stress in the aneurysm area. Blood flow has pulsatile characteristics. The current study employed a steady flow for analysis, but this model should not mitigate the value of the results shown herein since different studies have shown that steady flow provides a strong indication of fundamental hemodynamic trends that are present under both steady and pulsatile conditions in the aneurysm [36,37].

All the results presented were captured for only the central coronal plane (XY plane) of the aneurysm. Planar PIV was used in this study to capture the fluid dynamics and could not capture the out-of-plane component of the velocity. While it was expected to observe a complex flow in the XZ plane, the out-of-plane behavior of the flow remains ambiguous for future studies. If the out-of-plane velocity and transverse secondary flow development are deemed necessary, stereo-PIV, tomographic PIV [38,39], or three-dimensional phase-contrast MRI can be utilized [40]. These may be employed in future studies to help verify the results presented herein.

5. Conclusions

eCLIPs has undergone three iterations for the treatment of intracranial bifurcation aneurysms, the first never achieving clinical uptake due to the delivery impediments associated with its balloon-expandable stainless steel design. The second generation, the eCLIPs eBRS, with self-expanding nitinol, showed a calculable flow diversion effect at a bifurcation. A third generation has improved delivery characteristics and compatibility with smaller catheters. A fourth generation, the eBFD, was developed to build upon these improvements and also to try to achieve a sufficient flow diversion effect to obviate the need for adjunctive coiling. This study used PIV to measure the flow-diverting hemodynamics, implied by reducing the velocity in the aneurysm sac, in successive eCLIPs versions in comparison with a clinically recognized flow diverter, the PED, used as a reference predicate. The results showed that for various eCLIPs iterations, increasing metal coverage density was proportional to a reduction of the mean and maximum velocity in the aneurysm sac. The PED was not only less effective as a flow diverter in the bifurcation configuration than the eBFD, but also less effective at a bifurcation than in a sidewall configuration. The eBFD (fourth generation) showed equivalent flow diversion at a bifurcation to PED in sidewall anatomy. Thus, it was concluded that the eBFD has the potential for sufficient flow diversion and thrombosis in a bifurcation aneurysm without the need for adjunctive coiling. This thesis must be validated by clinical studies. The study also demonstrated the efficacy of the PIV measurement technique in assessing implant flow diversion and associated hemodynamics.

References

1. Jung, K.-H. New Pathophysiological Considerations on Cerebral Aneurysms. *Neurointervention* **2018**, *13*, 73–83. [CrossRef] [PubMed]

2. Foundation, B.A. Statistics and Facts—Brain Aneurysm Foundation. Available online: https://bafound.org/about-brain-aneurysms/brain-aneurysm-basics/brain-aneurysm-statistics-and-facts/ (accessed on 9 October 2020).

3. Shapiro, M.; Becske, T.; Sahlein, D.; Babb, J.; Nelson, P.K. Stent-supported aneurysm coiling: A literature survey of treatment and follow-up. *Am. J. Neuroradiol.* **2012**, *33*, 159–163. [CrossRef] [PubMed]

4. Johnston, S.C.; Dowd, C.F.; Higashida, R.T.; Lawton, M.T.; Duckwiler, G.R.; Gress, D.R. Predictors of rehemorrhage after treatment of ruptured intracranial aneurysms: The Cerebral Aneurysm Rerupture After Treatment (CARAT) study. *Stroke* **2008**, *39*, 120–125. [CrossRef] [PubMed]

5. Wanke, I.; Forsting, M. Stents for intracranial wide-necked aneurysms: More than mechanical protection. *Neuroradiology* **2008**, *50*, 991–998. [CrossRef]

6. Wong, G.K.C.; Kwan, M.C.L.; Ng, R.Y.T.; Yu, S.C.H.; Poon, W.S. Flow diverters for treatment of intracranial aneurysms: Current status and ongoing clinical trials. *J. Clin. Neurosci.* **2011**, *18*, 737–740. [CrossRef]

7. Jankowitz, B.T.; Thomas, A.; Jovin, T.; Horowitz, M. Y stenting using kissing stents for the treatment of bifurcation aneurysms. *J. Neurointerv. Surg.* **2012**, *4*, 16–21. [CrossRef]

8. Darkhabani, Z.M.; Lazzaro, M.A.; Zaidat, O.O. Pericallosal artery aneurysm treatment using Y-configuration stent-assisted coil embolization: A report of four cases. *J. Neurointerv. Surg.* **2012**, *4*, 459–462. [CrossRef]

9. Tang, A.Y.S.; Chung, W.C.; Liu, E.T.Y.; Qu, J.Q.; Tsang, A.C.O.; Leung, G.K.K.; Leung, K.M.; Yu, A.C.H.; Chow, K.W. Computational Fluid Dynamics Study of Bifurcation Aneurysms Treated with Pipeline Embolization Device: Side Branch Diameter Study. *J. Med. Biol. Eng.* **2015**, *35*, 293–304. [CrossRef]

10. Arthur, A.S.; Molyneux, A.; Coon, A.L.; Saatci, I.; Szikora, I.; Baltacioglu, F.; Sultan, A.; Hoit, D.; Almandoz, J.E.D.; Elijovich, L. The safety and effectiveness of the Woven EndoBridge (WEB) system for the treatment of wide-necked bifurcation aneurysms: Final 12-month results of the pivotal WEB Intrasaccular Therapy (WEB-IT) Study. *J. Neurointerv. Surg.* **2019**, *11*, 924–930. [CrossRef]

11. De Vries, J.; Boogaarts, H.D.; Sørensen, L.; Holtmannspoetter, M.; Benndorf, G.; Turowski, B.; Bohner, G.; Derakhshani, S.; Navasa, C.; van Zwam, W.H. eCLIPs bifurcation remodeling system for treatment of wide neck bifurcation aneurysms with extremely low dome-to-neck and aspect ratios: A multicenter experience. *J. Neurointerv. Surg.* **2020**. [CrossRef]

12. Caroff, J.; Mihalea, C.; Ikka, L.; Ozanne, A.; Gallas, S.; Chalumeau, V.; Moret, J.; Spelle, L. O-009 WEB shape modification during follow-up: The bicêtre experience. *J. Neurointerv. Surg.* **2020**. [CrossRef]

13. Chiu, A.H.; De Vries, J.; O'Kelly, C.J.; Riina, H.; McDougall, I.; Tippett, J.; Wan, M.; De Oliveira Manoel, A.L.; Marotta, T.R. The second-generation eCLIPs Endovascular Clip System: Initial experience. *J. Neurosurg.* **2018**, *128*, 482–489. [CrossRef] [PubMed]

14. Peach, T.W.; Ricci, D.; Ventikos, Y. A Virtual Comparison of the eCLIPs Device and Conventional Flow-Diverters as Treatment for Cerebral Bifurcation Aneurysms. *Cardiovasc. Eng. Technol.* **2019**, *10*, 508–519. [CrossRef] [PubMed]

15. Augsburger, L.; Farhat, M.; Reymond, P.; Fonck, E.; Kulcsar, Z.; Stergiopulos, N.; Rüfenacht, D.A. Effect of flow diverter porosity on intraaneurysmal blood flow. *Clin. Neuroradiol.* **2009**, *19*, 204–214. [CrossRef] [PubMed]

16. Liou, T.M.; Li, Y.C. Effects of stent porosity on hemodynamics in a sidewall aneurysm model. *J. Biomech.* **2008**, *41*, 1174–1183. [CrossRef] [PubMed]

17. Roszelle, B.N.; Gonzalez, L.F.; Babiker, M.H.; Ryan, J.; Albuquerque, F.C.; Frakes, D.H. Flow diverter effect on cerebral aneurysm hemodynamics: An in vitro comparison of telescoping stents and the Pipeline. *Neuroradiology* **2013**, *55*, 751–758. [CrossRef]

18. Dennis, K.D.; Rossman, T.L.; Kallmes, D.F.; Dragomir-Daescu, D. Intra-aneurysmal flow rates are reduced by two flow diverters: An experiment using tomographic particle image velocimetry in an aneurysm model. *J. Neurointerv. Surg.* **2015**, *7*, 937–942. [CrossRef]

19. Marotta, T.R.; Gunnarsson, T.; Penn, I.; Ricci, D.R.; McDougall, I.; Marko, A.; Bourne, G.; Da Costa, L. A novel endovascular clip system for the treatment of intracranial aneurysms: Technology, concept, and initial experimental results: Laboratory investigation. *J. Neurosurg.* **2008**, *108*, 1230–1240. [CrossRef]
20. O'Kelly, C.; Rempel, J.L.; Diestro, J.D.B.; Marotta, T.R. Letter to the Editor: Pandemic (COVID-19) Proctoring for eCLIPs Neurointervention. *World Neurosurg.* **2020**, *142*, 575. [CrossRef]
21. Dholakia, R.; Sadasivan, C.; Fiorella, D.J.; Woo, H.H.; Lieber, B.B. Hemodynamics of flow diverters. *J. Biomech. Eng.* **2017**, *139*, BIO-16-1270. [CrossRef]
22. Yazdi, S.G.; Huetter, L.; Docherty, P.D.; Williamson, P.N.; Clucas, D.; Jermy, M.; Geoghegan, P.H. A Novel Fabrication Method for Compliant Silicone Phantoms of Arterial Geometry for Use in Particle Image Velocimetry of Haemodynamics. *Appl. Sci.* **2019**, *9*, 3811. [CrossRef]
23. Geoghegan, P.H.; Buchmann, N.A.; Spence, C.J.T.; Moore, S.; Jermy, M. Fabrication of rigid and flexible refractive-index-matched flow phantoms for flow visualisation and optical flow measurements. *Exp. Fluids* **2012**, *52*, 1331–1347. [CrossRef]
24. Johnston, I.D.; McCluskey, D.K.; Tan, C.K.L.; Tracey, M.C. Mechanical characterization of bulk Sylgard 184 for microfluidics and microengineering. *J. Micromech. Microeng.* **2014**, *24*, 35017. [CrossRef]
25. Yousif, M.Y.; Holdsworth, D.W.; Poepping, T.L. A blood-mimicking fluid for particle image velocimetry with silicone vascular models. *Exp. Fluids* **2011**, *50*, 769–774. [CrossRef]
26. Blanco, P.J.; Watanabe, S.M.; Dari, E.A.; Passos, M.A.R.F.; Feijóo, R.A. Blood flow distribution in an anatomically detailed arterial network model: Criteria and algorithms. *Biomech. Model. Mechanobiol.* **2014**, *13*, 1303–1330. [CrossRef] [PubMed]
27. Briganti, F.; Leone, G.; Marseglia, M.; Mariniello, G.; Caranci, F.; Brunetti, A.; Maiuri, F. Endovascular treatment of cerebral aneurysms using flow-diverter devices: A systematic review. *Neuroradiol. J.* **2015**, *28*, 365–375. [CrossRef]
28. Mut, F.; Raschi, M.; Scrivano, E.; Bleise, C.; Chudyk, J.; Ceratto, R.; Lylyk, P.; Cebral, J.R. Association between hemodynamic conditions and occlusion times after flow diversion in cerebral aneurysms. *J. Neurointerv. Surg.* **2015**, *7*, 286–290. [CrossRef]
29. Yu, C.H.; Matsumoto, K.; Shida, S.; Kim, D.J.; Ohta, M. A steady flow analsys on a cerebral aneurysm model with several stents for new stent design using PIV. *J. Mech. Sci. Technol.* **2012**, *26*, 1333–1340. [CrossRef]
30. Castro, M.A.; Putman, C.M.; Cebral, J.R. Computational fluid dynamics modeling of intracranial aneurysms: Effects of parent artery segmentation on intra-aneurysmal hemodynamics. *Am. J. Neuroradiol.* **2006**, *27*, 1703–1709.
31. Fiorella, D.; Arthur, A.S.; Chiacchierini, R.; Emery, E.; Molyneux, A.; Pierot, L. How safe and effective are existing treatments for wide-necked bifurcation aneurysms? Literature-based objective performance criteria for safety and effectiveness. *J. Neurointerv. Surg.* **2017**, *9*, 1197–1201. [CrossRef]
32. Kim, Y.H.; Xu, X.; Lee, J.S. The effect of stent porosity and strut shape on saccular aneurysm and its numerical analysis with lattice Boltzmann method. *Ann. Biomed. Eng.* **2010**, *38*, 2274–2292. [CrossRef] [PubMed]
33. Najjari, M.R.; Hinke, J.A.; Bulusu, K.V.; Plesniak, M.W. On the rheology of refractive-index-matched, non-Newtonian blood-analog fluids for PIV experiments. *Exp. Fluids* **2016**, *57*, 96. [CrossRef]
34. Frolov, S.V.; Sindeev, S.V.; Liepsch, D.; Balasso, A. Experimental and CFD flow studies in an intracranial aneurysm model with Newtonian and non-Newtonian fluids. *Technol. Health Care* **2016**, *24*, 317–333. [CrossRef] [PubMed]
35. Valencia, A.; Zarate, A.; Galvez, M.; Badilla, L. Non-Newtonian blood flow dynamics in a right internal carotid artery with a saccular aneurysm. *Int. J. Numer. Methods Fluids* **2006**, *50*, 751–764. [CrossRef]
36. Babiker, M.H.; Gonzalez, L.F.; Albuquerque, F.; Collins, D.; Elvikis, A.; Zwart, C.; Roszelle, B.; Frakes, D.H. An in vitro study of pulsatile fluid dynamics in intracranial aneurysm models treated with embolic coils and flow diverters. *IEEE Trans. Biomed. Eng.* **2012**, *60*, 1150–1159. [CrossRef] [PubMed]
37. Nair, P.; Chong, B.W.; Indahlastari, A.; Ryan, J.; Workman, C.; Babiker, M.H.; Farsani, H.Y.; Baccin, C.E.; Frakes, D. Hemodynamic characterization of geometric cerebral aneurysm templates treated with embolic coils. *J. Biomech. Eng.* **2016**, *138*, 021011. [CrossRef]
38. Nguyen, Y.N.; Kabinejadian, F.; Ismail, M.; Kong, W.K.F.; Tay, E.L.W.; Leo, H.L. Ex vivo assessment of bicuspidization repair in treating severe functional tricuspid regurgitation: A stereo-scopic PIV study. *Sci. Rep.* **2019**, *9*, 11504. [CrossRef]

39. Medero, R.; Ruedinger, K.; Rutkowski, D.; Johnson, K.; Roldán-Alzate, A. In Vitro Assessment of Flow Variability in an Intracranial Aneurysm Model Using 4D Flow MRI and Tomographic PIV. *Ann. Biomed. Eng.* **2020**, *48*, 2484–2493. [CrossRef]

40. Yamashita, S.; Isoda, H.; Hirano, M.; Takeda, H.; Inagawa, S.; Takehara, Y.; Alley, M.T.; Markl, M.; Pelc, N.J.; Sakahara, H. Visualization of hemodynamics in intracranial arteries using time-resolved three-dimensional phase-contrast MRI. *J. Magn. Reson. Imaging Off. J. Int. Soc. Magn. Reson. Med.* **2007**, *25*, 473–478. [CrossRef]